Nanoscale

PAPER

View Article Online
View Journal | View Issue

Cite this: *Nanoscale*, 2017, **9**, 16459

Sensitive and specific detection of explosives in solution and vapour by surface-enhanced Raman spectroscopy on silver nanocubes†

Sultan Ben-Jaber,[a] William J. Peveler,[a] Raul Quesada-Cabrera,[a] Christian W. O. Sol,[b] Ioannis Papakonstantinou[b] and Ivan P. Parkin*[a]

Received 12th July 2017,
Accepted 11th October 2017

DOI: 10.1039/c7nr05057g

rsc.li/nanoscale

Surface-enhanced Raman spectroscopy (SERS) has been widely utilised as a sensitive analytical technique for the detection of trace levels of organic molecules. The detection of organic compounds in the gas phase is particularly challenging due to the low concentration of adsorbed molecules on the surface of the SERS substrate. This is particularly the case for explosive materials, which typically have very low vapour pressures, limiting the use of SERS for their identification. In this work, silver nanocubes (AgNCs) were developed as a highly sensitive SERS substrate with very low limit-of-detection (LOD) for explosive materials down to the femtomolar (10^{-15} M) range. Unlike typical gold-based nanostructures, the AgNCs were found suitable for the detection of both aromatic and aliphatic explosives, enabling detection with high specificity at low concentration. SERS studies were first carried out using a model analyte, Rhodamine-6G (Rh-6G), as a probe molecule. The SERS enhancement factor was estimated as 8.71×10^{10} in this case. Further studies involved femtomolar concentrations of 2,4-dinitrotoluene (DNT) and nanomolar concentrations of 1,3,5-trinitroperhydro-1,3,5-triazine (RDX), as well as vapour phase detection of DNT.

Introduction

Surface-enhanced Raman spectroscopy (SERS) is a powerful technique for the sensitive and selective detection of ultra-trace levels of a wide range of organic molecules, including explosives, biomolecules and environmental pollutants.[1–3] In SERS, the intensity of the Raman signal is enhanced upon intensification of an electric field (E-field) at the surface of a nanometallic structure.[1] In practise, an analytical enhancement factor (AEF) is conveniently defined as indicated in eqn (1), where I_{SERS} and I_{RS} are the intensity of the average SERS and conventional Raman signal respectively, and C_R and C_{SERS} are the analyte concentrations in the Raman and SERS measurements respectively.

$$\mathrm{AEF} = \frac{I_{SERS} \times C_{RS}}{I_{RS} \times C_{SERS}} \quad (1)$$

This analytical enhancement factor (AEF) is typically of the order of 10^4–10^{10}. A wide range of materials have been used for construction of SERS substrates, with particular attention to those containing noble metal nanoparticles that display plasmonic bands, such as gold (AuNPs) and silver (AgNPs).[4,5] Resonance excitation of localised free electrons in metallic particles causes collective oscillation (localised surface plasmon resonance – LSPR), enhancing surface polarisation and thus contributing to promote the Raman scattering intensity. It is interesting to note that AgNPs show a remarkable LSPR effect over other noble metals, with quality factors (Q_{LSPR}) estimated to be 97.43, compared to that of AuNPs (33.99).[6] The enhancement field surrounding the metal nanoparticle may extend several nanometres from the nanoparticle surface.[7–10]

In the particular case of the detection of explosives in solution, a range of noble metal-based SERS substrates have been used, including thin films of noble metal nanostructures and composites of noble metals with transition metals or semiconductors.[11–13] Recently, Jamil *et al.* detected femtomolar levels (100 fM) of trinitrotoluene (TNT) with high reproducibility using a substrate consisting of gold nanostructures deposited on a flat gold disc.[14] Others have detected extremely ultra-trace concentrations of TNT using *p*-aminothiophenol-functionalized AgNPs supported on graphene nanosheets, however the analyte signals were overlapped by the very strong SERS signals of the aminothiophenol, severely hampering sen-

[a]*Department of Chemistry, Materials Chemistry Centre, University College London, 20 Gordon St., London WC1H 0AJ, UK. E-mail: i.p.parkin@ucl.ac.uk*
[b]*Department of Electronic and Electrical Engineering, University College London, Torrington Place, London WC1E 7JE, UK*

†Electronic supplementary information (ESI) available: Additional Raman spectra and tables, Ag nanosphere synthesis and further modelling details. See DOI: 10.1039/c7nr05057g

sitivity and specificity.[15] Detection of small signals from low concentration DNT (10^{-13} M) was demonstrated by Demeritte *et al.* using gold-functionalised single-walled carbon nanotubes, however the nature of the signals meant that specificity was low.[16] Finally Kleinman *et al.* previously detected RDX from a 500 nM solution, also using gold-functionalised single-walled carbon nanotubes but again with poor specificity as only one band at around 1600 cm^{-1} was observed.[17] In a study by Chen *et al.*, RDX was detected using a monolayer of AuNPs, with a limit of detection (LOD) of 0.19 ppm (*ca.* 9×10^{-7} M).[18]

To extend the utility of the SERS detection of explosives, vapour sensing for 'stand off' detection has also been tested.[19,20] For instance, Emamian *et al.* fabricated a substrate consisting on AgNPs 'ink' on a sheet of polyethylene terephthalate for detection of DNT from the vapour phase.[21] Another study by Tamane *et al.* demonstrated vapour phase detection of nitro-explosives by using AgNPs on Si where they enclosed the substrate in a sealed tube with explosive simulant at thermodynamic equilibrium.[22] They concluded that desorption and decomposition of TNT in the vapour phase hindered detection by SERS, as they observed SERS enhancement after 10 seconds followed by a decreasing signal intensity over time with splitting of several key Raman bands. In previous work, we have measured SERS of TNT in the vapour phase using a fabricated substrate consisting on a TiO_2 thin film decorated with AuNPs.[23] The substrate was pre-activated by UV radiation prior exposure to TNT vapours and the SERS spectrum was recorded with good specificity.

Further engineering of SERS substrates requires a good distribution of hotspots for the enhancement of weak Raman signals.[24–26] These hotspots result from close spacing between two or more metal nanoparticles.[27,28] The location of molecules in hotspots and the estimation of the number of molecules probed are often hampered by surface roughness and the irregular microstructure of most SERS substrates.[24,29] The enhancement factor (EF) values in SERS crucially depends on the physical properties of the substrate (particle size and shape). A strong enhancement has been observed from substrates containing regular-shaped nanoparticles with sharp faces or tips (nanocubes, nanorods, *etc.*) compared to that induced by spherical particles.[30–34]

Silver nanocubes (AgNCs) have been previously used to detect a range of Raman reporters such as 4-methylbenzenethiol (4-MBT),[35] as well as pesticides[36] and explosive binders.[37] Here we tackle the more challenging problem of direct explosives detection at trace levels. Two relevant analytes are focussed on – 2,4-dinitrotoluene (DNT) and cyclotrimethylenetrinitramine (RDX). DNT is a contaminant and the main decomposition product of trinitrotoluene (TNT) and can be used as a detection marker for landmines and other explosive compositions.[20] The detection of DNT is challenging due to its low vapour pressure at room temperature (0.035 Pa at 25 °C), but it is still more concentrated than TNT in the vapour phase.[38] RDX is one of the most potent secondary explosives and it is found in compositions such as Semtex. The vapour pressure of RDX is around 4.4×10^{-7} Pa at 25 °C, making vapour detection very difficult.[39,40]

In this work, we use silver nanocubes (AgNCs) as a highly sensitive SERS substrate with very low limit-of-detection (LOD). We detect ultra-trace concentrations of explosives in the femtomolar range (10^{-15} M) in solution and vapour, as well as a model analyte, Rhodamine-6G (Rh-6G), with excellent enhancement factors (>10^9). Modelling of the electromagnetic response of the particles was investigated using a finite difference time domain (FDTD) approach to calculate the E-field around the AgNCs.[35,41] These calculations are consistent with the strong enhancement observed in our experiments and demonstrate the potential for AgNCs in SERS substrate fabrication. Our EF values for RDX and DNT in particular are some of the highest achieved, with the best spectral specificity (*i.e.* characteristic spectral features are identified unequivocally).

Experimental

All chemicals were purchased from Sigma-Aldrich and used as received. Silver nitrate ($AgNO_3$, 99%), poly-vinyl pyrrolidone (PVP, $M_w \approx 55\,000$), sodium sulphide (Na_2S, 98%), ethylene glycol (EG) anhydrous (99.8%), acetone (reagent grade) and ethanol (reagent grade) were used in the synthesis of AgNCs. All aqueous solutions were prepared using deionized water (18.3 MΩ cm). Rhodamine-6G (99%), 2,4-dinitrotoluene (DNT) (97%) and RDX (analytical sample provided as a gift) were analytes in the SERS experiments. Samples were dried under a stream of nitrogen to recrystallize the solid explosive for original Raman measurements as a reference. The samples were dispersed in ethanol to different dilution concentrations for the SERS experiments.

Preparation of silver nanocubes (AgNCs)

AgNCs were prepared using the polyol method.[42,43] In a typical procedure, 10 mL of ethylene glycol (EG) was heated with stirring at 150 °C for 1 hour. A Na_2S solution (80 μL, 3 mM) was then added and after 8–9 min, a 1.5 mL solution of PVP (30 mg, 0.27 mmol by monomer mass) in EG and 0.5 mL of $AgNO_3$ (24 mg, 0.14 mmol) in EG were added simultaneously over the course of 8 minutes, with vigorous stirring. This was followed immediately by a further 3 mL of EG. The reaction was completed in 25 min and the mixture appeared ochre-green. The product was cooled, washed with acetone and centrifuged at 3000 rpm for 25 min, then the pelletized product was re-dispersed in DI water followed by washing twice more, to remove excess EG and PVP. Finally the precipitate was dispersed in 3 mL deionised water for further analysis.

Preparation of SERS substrate

AgNCs and analyte samples were drop-cast onto borosilicate glass slides either sequentially or as an intimate mixture of the two solutions. The latter was found the most efficient method for the SERS detection of explosives. In this procedure, 100 μL of ethanolic analyte solutions at the given concentrations were

mixed with 100 μL of the AgNCs in ethanol, under strong stirring conditions for 20 min. The mixtures were then centrifuged and the residual pellet, drop-cast onto borosilicate glass and left to dry in air for few minutes prior to SERS measurements.

Vapour detection measurements

A microscope slide coated with AgNCs was exposed to DNT vapours (100 mg) in a water bath at 25, 30 and 40 °C, during different time periods (1–3 minutes). Raman studies were carried out immediately after each exposure period.

Characterisation techniques

Raman spectroscopy studies were carried out using a Renishaw 1000 spectrometer coupled to a microscope with 50× objective lens and equipped with a 633 nm laser (1.9 eV, 1.0 mW). The laser spot size was *ca.* 4.4 μm^2. The Raman system was calibrated using a silicon reference. The acquisition time was 10 s with a single accumulation for all measurements. X-ray diffraction (XRD) analysis was performed using a Bruker-AXS D8 diffractometer system. The instrument operates with a Cu X-ray source, monochromated (λ = 1.54 Å) and the incident beam angle was 1°. UV/vis spectroscopy was carried out using a PerkinElmer Lambda 25 UV/Vis/NIR instrument. Scanning electron microscopy (SEM) and energy-dispersive X-ray spectroscopy (EDX) were carried out using a Jeol JSM-6700F. Transmission electron microscopy (TEM) images and selected area electron diffractograms (SAEDs) were obtained using a high resolution TEM Jeol 2100 with a LaB-6 source operating at an acceleration voltage of 200 kV. Micrographs were recorded on a Gatan Orius camera.

Results and discussion

AgNCs were prepared using the polyol method adapted from the literature.[42,43] Ethylene glycol (EG) was used as a solvent and reducing agent. The reaction takes place in the presence of sodium sulphide (Na_2S), which restricts the formation of Ag metal seeds and controls the growth of silver particles into random shapes. At the same time PVP induces the formation of AgNCs *via* binding to the silver ⟨100⟩ facets. This synthesis rendered a large population (>74%) of AgNCs with average side length of 153 nm ± S.D. of 25 nm (N = 137) for the nanocubes (Fig. 1). The AgNC colloidal suspension was stirred, centrifuged to concentrate the nanoparticles, and drop-cast onto borosilicate glass slides. The centrifugation encouraged the formation of AgNCs clusters and increases the hotspot population across the film. SEM studies on these AgNC substrates (Fig. S7†) revealed the remainder of the particles consisted of rod-like and triangular silver NPs. ESI Fig. S4† shows size distribution histogram of AgNCs on a substrate. XRD analysis (Fig. 2a) showed diffraction peaks corresponding to [111], [200] and [220] planes, which are representative of cubic elemental silver. The presence of the [200] peak at 44° (2θ) confirmed the preferred orientation growth of the nanocubes. The characteristic surface plasmon resonance (SPR) absorbance maximum of the AgNCs was observed at λ = 444 nm in solution and broadened and red shifted to 460 nm when deposited on the substrate, due to a change in dielectric medium and aggregation of the particles (Fig. 2b).

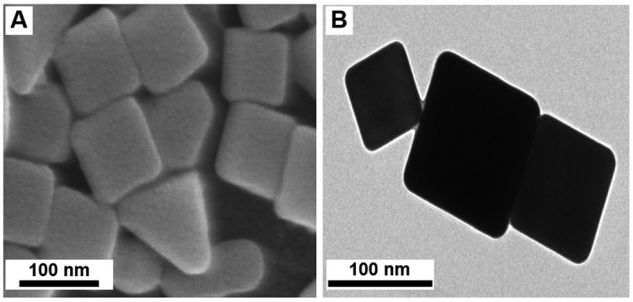

Fig. 1 (a) Scanning electron microscopy (SEM) and (b) transmission electron microscopy (TEM) images of AgNCs.

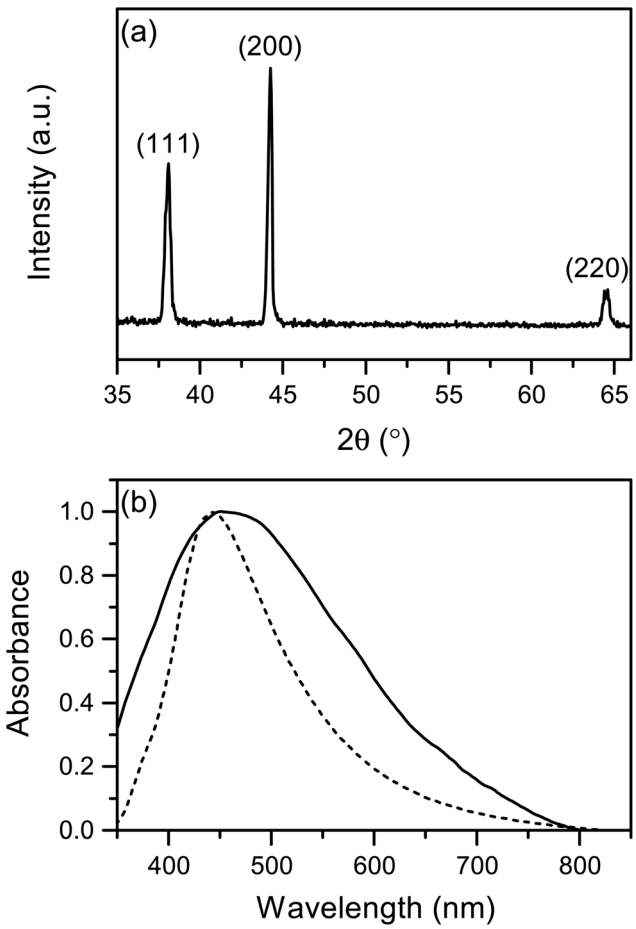

Fig. 2 (a) XRD pattern of the AgNCs sample showing the typical face-centred cubic structure of silver; (b) normalised UV/Vis spectrum of AgNCs in solution (dashed line) and as-deposited (solid line) on a glass substrate, showing the surface plasmon resonance (SPR) absorption bands at λ_{max} = 444 and 460 nm, respectively.

The efficiency of this substrate was initially evaluated using different concentrations of Rhodamine 6G (Rh-6G), namely 10^{-7}, 10^{-9} and 10^{-12} M (Fig. 3). Rh-6G is widely used as a standard in SERS and has an absorption band at 528 nm, which is not in resonance with the laser source used in our experiments (633 nm),[44] however it has a conveniently large Raman cross-section ($d\sigma/d\Omega$) of *ca.* 1×10^{-27} cm^2 sr^{-1} (*ca.* 1×10^{-18} cm^2 sr^{-1} for single molecule SM-SERS).[44] SERS enhancement was observed, demonstrating that analytes can bind to the cubes, despite the PVP surfactant, and Fig. 3a shows SERS spectra of the dye with characteristic bands at 611 cm^{-1} (C–C–C ring in-plane bend), 769 cm^{-1} (C–H out-of-plane bend), 1183 cm^{-1} (C–H in-plane bend), 1311 cm^{-1} (C–O–C stretch), and 1361, 1511, 1649 cm^{-1} (aromatic C–C stretch), which are all clearly observed even at low concentrations (10^{-12} M). No PVP Raman modes were observed as the silver cubes were washed with acetone and water to insure a removal of PVP and EG residue. Comparison among Raman and SERS bands of Rh-6G are given in Table S1.† Mapping of the substrate surface (Fig. 3b and S6†) also showed good reproducibility and enhancement of Raman signals at all analysis points, which indicated an efficient distribution of hotspots. Close inspection of Fig. 3b shows differences in band intensities, particularly for the band at 611 cm^{-1}, which has been attributed to different orientations of the Rh-6G molecules adsorbed to the region near the hotspots. The average EF for a slightly more consistent 10^{-7} M sample (Fig. S6†) was estimated was between 8.71×10^{10} and 1.19×10^{11} (see ESI Table S2†).

The strong enhancement was not only attributed to particle shape but also size, as the size nanoparticles also plays a role in the enhancement factor. Under identical measurements conditions, larger nanoparticles enhance Raman signals more than smaller.[35] Therefore, the large size of the AgNCs produced in this work has contributed in the strong enhancement, and we decided to probe this further with FDTD modelling.

Enhancement mechanism of the AgNCs substrate

Insight into the nature of the enhancement of the AgNCs as a SERS substrate was sought using a commercial-grade simulator based on the finite-difference time-domain method (Lumerical-FDTD). These studies calculated and compared the electric field intensity ($|E|^2$) around AgNCs and silver nanospheres (AgNSs) on a glass substrate relative to the incident intensity ($|E|^2_{inc}$) when illuminated with a 633 nm source (Fig. 4). From inspection of Fig. 4b, it can be observed that the AgNCs show a high E-field localised at the corners of the cube

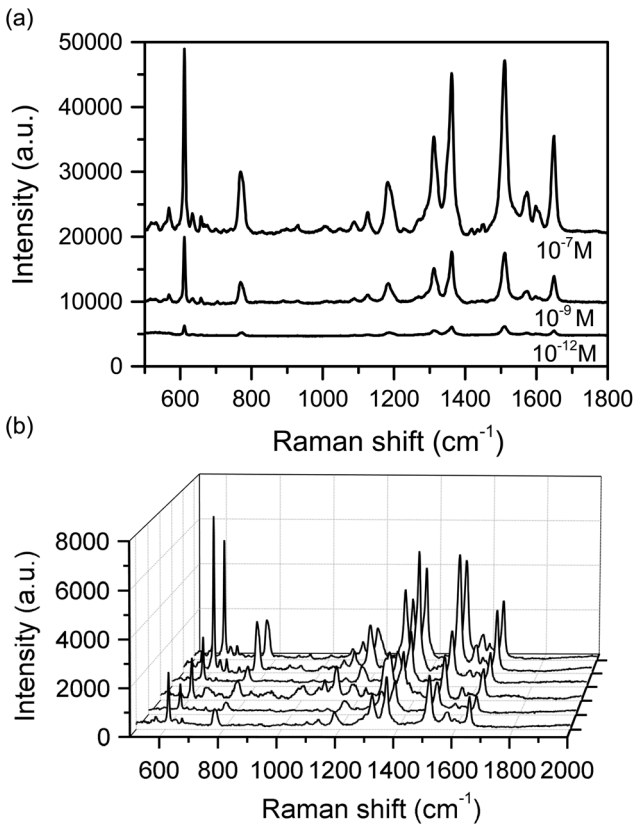

Fig. 3 (a) SERS spectra of Rh-6G on a AgNCs substrate. The Rh-6G was deposited from different ethanolic solutions (10^{-7} M, 10^{-9} M and 10^{-12} M). (b) Mapping of SERS spectra of Rh-6G from a 10^{-9} M solution across a AgNCs substrate.

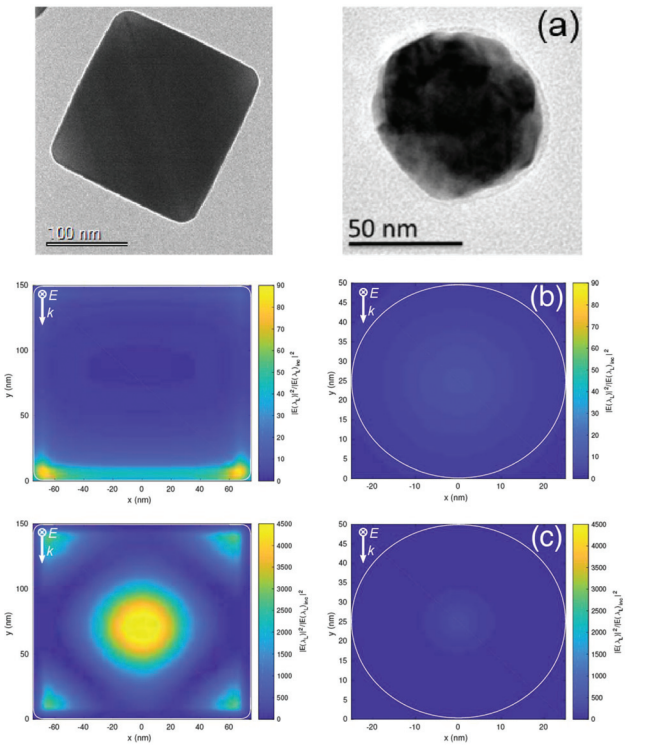

Fig. 4 (a) TEM images of a silver nanocube (AgNC) and a silver round nanoparticle (AgNS); (b) comparison of maximum and mean electric field enhancement ($|E|^2/|E|^2_{inc}$) at the surface of the particles for singular AgNC (max = 88.3; mean = 8.74) and AgNS (max = 7.56; mean 2.91); (c) comparison maximum and mean electric field enhancements in between dimer AgNCs (max = 4820; mean 801.6) and AgNSs (max = 237; mean = 20.6) with 4 nm spacing due to the surrounding dielectric coating. Edge of particle delineated in white.

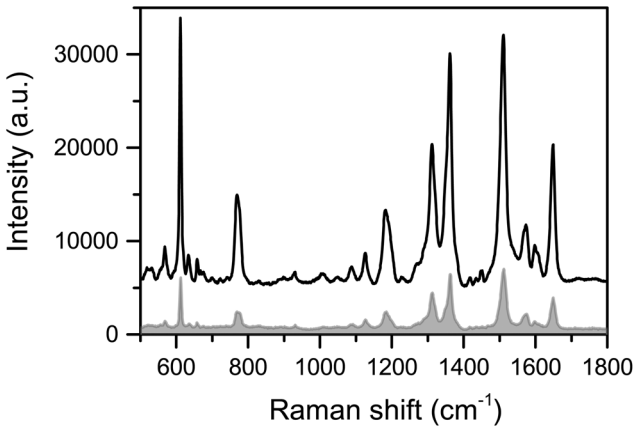

Fig. 5 SERS spectra of Rh-6G from a 10^{-7} M ethanolic solution on AgNCs (black line) and AgNSs (grey line) substrates.

at the interface with the substrate, compared with that from AgNSs, which is relatively weak and spread over a larger area of the particle surface. The simulations also investigated the E-field enhancement in between two particles separated by 2 nm thick dielectric coatings (n = 1.5) for both AgNCs and AgNSs (Fig. 4c). The results further supported the E-field confinement within AgNCs, showing significant intensity compared to that within AgNSs gaps. These calculations agreed with our experimental observations when comparing SERS studies of Rh-6G using AgNC and AgNS substrates. As evidenced in Fig. 5, for the same concentration of the analyte, the Raman features of Rh-6G were dramatically enhanced on the AgNCs substrate, with an EF of 8.71×10^{10}, where 8.94×10^{9} was estimated for the same level of Rh-6G with AgNSs. Fig. S6† shows multiple spot measurements on a solution of 10^{-7} M Rh-6G across the AgNCs substrate, demonstrating good point-to-point reproducibility.

It is worth noting that the FDTD simulations consider only the electromagnetic enhancement and ignore the potential charge transfer mechanism between AgNCs and analyte molecules. The chemisorption of the analyte onto the sharp corners and edges of AgNCs (where there is a strong, localised E-field) may induce changes in the molecule polarizability and thus contribute to the total spectral enhancement of the analyte.[45] Typically, the chemical enhancement contributes to an increase in intensity of a few orders of magnitude over the overall enhancement, whereas the electromagnetic contribution is often over 10^{10}. The presence of selectively-enhanced bands in the spectra suggests an interaction of the π orbitals of the molecule with the metal surface.

Ultra-trace detection of explosives: DNT and RDX

The SERS detection of DNT was carried out using a range of solution concentrations (10^{-5}, 10^{-7}, 10^{-9}, 10^{-12} and 10^{-15} M) in ethanol deposited on the AgNCs substrate, following the procedure described in the Experimental section (*vide supra*). The corresponding SERS spectra are plotted in Fig. 6, showing

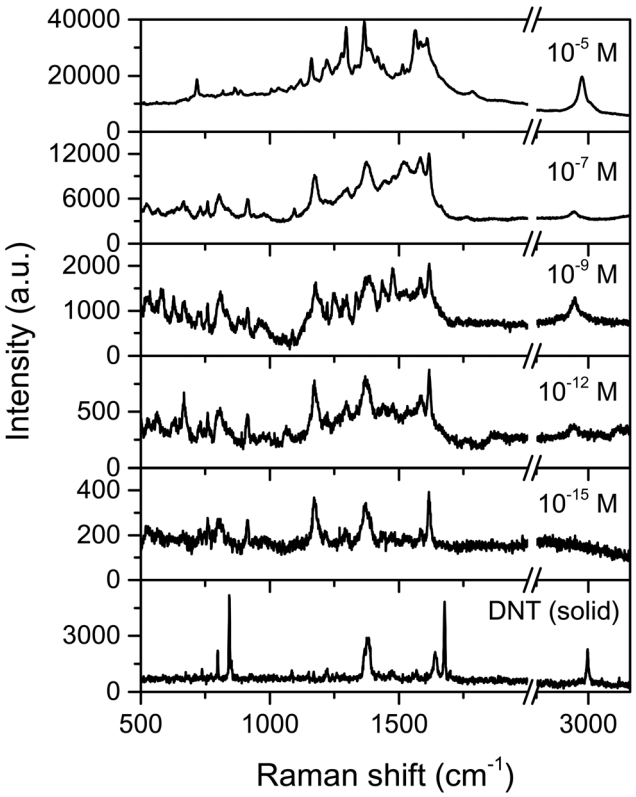

Fig. 6 Raman and SERS spectra of DNT deposited on AgNCs substrate from different concentrations in ethanol up to the femtomolar range. Bands at ~1350–1390 and 1560 cm^{-1} are assigned to symmetric and asymmetric stretching modes of NO_2 respectively, and bands at ~800 and 1170–1190 cm^{-1} are assigned to out-of-plane C–H and C–N, and in-plane H–C–C modes respectively. The band at 1615 cm^{-1} is attributed to stretching of aromatic ring-NO_2 and the band at high frequency ~2995 cm^{-1} is attributed to aromatic C–H stretching mode.

characteristic Raman-active bands of DNT. It is worth noting that band shifting and the disappearance of some Raman bands are expected in the SERS studies due to surface selection rules and the influence of substrate geometry on vibrational and scattering processes. Only the characteristic modes of the moiety that is adsorbed on the metallic surface are enhanced and thus we may expect fewer bands in the SERS spectra compared to those in the conventional Raman spectrum.[5,46] The symmetric and asymmetric stretching modes of NO_2 were clearly observed in the regions of 1340–1380 cm^{-1} and 1520–1590 cm^{-1}, respectively. The strong NO_2 stretching band at 1356 cm^{-1} was shifted to 1360 cm^{-1} in the SERS spectra (Fig. 6). A very strong band at around 1615 cm^{-1} was assigned to the aromatic ring-NO_2 stretch and the bands around 1070–1090 cm^{-1} correspond to C–N–O bending modes. In-plane and out-of-plane C–H modes were detected at 1190 cm^{-1} and 790–800 cm^{-1}, respectively, as well as a medium band around 1100 cm^{-1}, which was assigned to the C–C stretch mode. The band at 2969 cm^{-1} was assigned to the asymmetric C–H vibration of the CH_3 group and it was particularly enhanced compared to that in the Raman spectrum of

DNT powder. Weak Raman bands such as 1270 cm^{-1} and 734 cm^{-1} were also strongly enhanced and shifted to 1290 cm^{-1} and 722 cm^{-1} respectively, in the SERS spectra.

The enhancement of all these bands was detected even for the lowest concentration of DNT within the femtomolar range (10^{-15} M), with average EF estimated as 1.28×10^{10}. Importantly, this low limit of detection was achieved with high spectral specificity.

The SERS and Raman spectra of RDX are shown in Fig. 7, from 10^{-5}, 10^{-7} and 10^{-9} M ethanol solutions deposited on a AgNCs substrate. The characteristic symmetric stretching mode of the ring (breathing) at 881 cm^{-1} was strongly enhanced even at nanomolar concentrations (10^{-9} M) (Fig. 7), and the EF for RDX on AgNCs was estimated to be 9.26×10^{10}. Moreover, additional bands at 935 cm^{-1} (ring stretching and N–O deformation) and those in the range of 1200–1350 cm^{-1} (N–N stretching, CH_2 scissoring and symmetric NO_2 stretching) were clearly observed at the lowest concentrations of RDX. ESI Fig. S2† shows the linear correlation between band intensity (band at 889 cm^{-1}) and sample concentration.

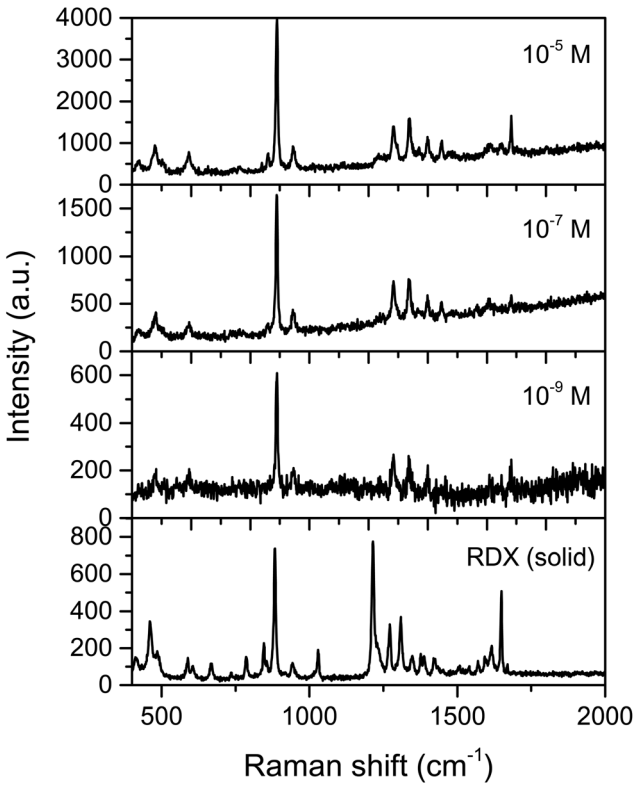

Fig. 7 Raman spectrum of neat RDX, and SERS spectra of 10^{-5}, 10^{-7}, 10^{-9} M of RDX on AgNCs. A sharp peak at ~881 cm^{-1} was strongly enhanced which corresponds to the symmetric ring-breathing mode, the band at 935 cm^{-1} attributed to ring stretching and N–O deformation. Bands at 1274 cm^{-1} for scissoring of CH_2 and stretching vibration of N–N, 1330 cm^{-1} attributed to CH_2 wagging, 1397 cm^{-1} asymmetric stretching NO_2 where the band at 1649 cm^{-1} is attributed to an asymmetric stretching of NO_2.

For both DNT and RDX, the results observed in this work represent a significant improvement compared to previous studies on SERS detection of explosives. Previous publications have achieved limits of detection of about 10^{-13} M for TNT and DNT[16,47] detection and 0.5×10^{-6} M of RDX,[17] however, those published methods show either low specificity or complicated spectra and we have improved on this with detection of 10^{-15} M of DNT and 10^{-9} M of RDX with clear observable fingerprint peaks, and thus high specificity, thanks to the AgNCs allowing for both improved LODs and improved spectral quality, facilitating easier explosive identification at low levels.

The identification of DNT was also carried out after exposing the AgNCs substrate to DNT vapour in a sealed container at 40 °C for 3 minutes (Fig. 8). The vapour pressure of DNT is estimated to be 1.78 ppm at 40 °C, which if saturated leads to effective concentration of *ca.* 9 μM,[48] although in reality the bound surface concentrations will be lower due to a short equilibration time. As Fig. 8b shows, several characteristic bands were observed and strongly enhanced, for instance, the bands at 1347–1357 cm^{-1}, that correspond to stretching modes of NO_2, as well as bands at low frequencies such as 791, 834 and 911 cm^{-1}. In addition, some bands (at 1269 and 1401 cm^{-1}) that correspond to typically weak Raman modes were strongly enhanced in the SERS study.

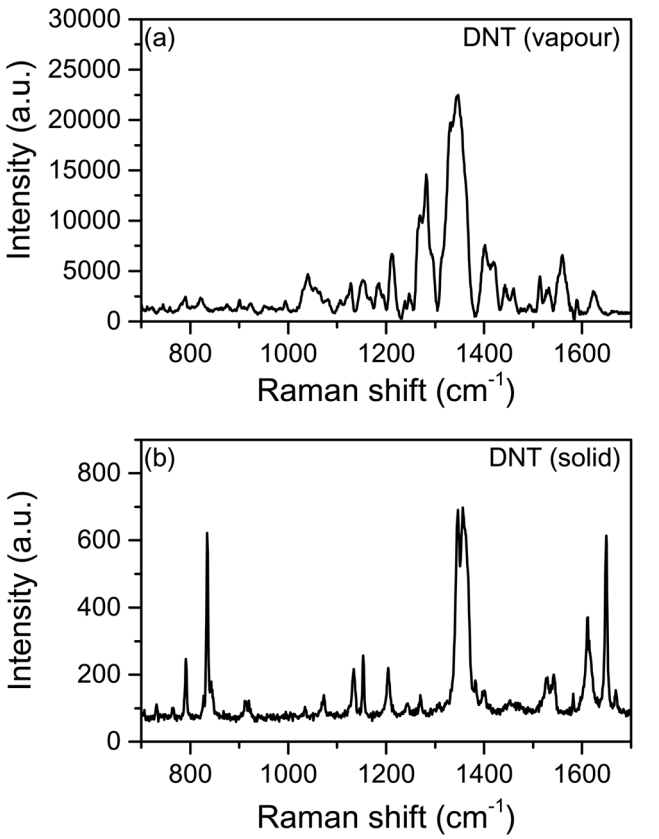

Fig. 8 (a) Raman spectrum of DNT powder, (b) SERS of DNT from a AgNCs substrate exposed to the explosive vapour at 40 °C for 3 min.

Conclusions

We have demonstrated a simple but sensitive SERS substrate based on AgNCs for the detection of ultra-trace concentrations of explosives. The substrate provided high sensitivity and specificity and allowed detection of femtomolar concentrations of DNT and vapour DNT, and nanomolar levels of RDX, two model explosive materials. The mechanism of the Raman enhancement is largely electromagnetic in nature, but using FDTD calculations of the E-field of the nanocubes in comparison to nanospheres, there is a suggestion chemical enhancement also plays a role. The SERS enhancement factor when using Rh-6G as a model molecule with high Raman cross-section was estimated at 8.71×10^{10}, and enhancement factors of 1.28×10^{10} and 9.26×10^{10} are given for DNT and RDX respectively, some of the highest reported, with excellent spectral resolution of key fingerprint regions. Optimisation of this system may have potential for stand-off detection of DNT and other explosive vapours, and our work will focus on improved signal collection and processing from homogenous arrays.

Conflicts of interest

There are no conflicts to declare.

Acknowledgements

SBJ acknowledges the support of the government of Saudi Arabia, Ministry of Interior, King Fahd Security College (KFSC), WJP acknowledges the EPSRC for funding (EP/M506448/1). The authors thank Dr Nadia Abdul-Karim (Canfield University) for provision of the RDX sample.

Notes and references

1 E. C. Le Ru, *Principles of surface-enhanced raman spectroscopy and related plasmonic effects*, Elsevier Science, Amsterdam, London, 2009.
2 A. Hakonen, P. O. Andersson, M. Stenbæk Schmidt, T. Rindzevicius and M. Käll, *Anal. Chim. Acta*, 2015, **893**, 1–13.
3 R. A. Halvorson and P. J. Vikesland, *Environ. Sci. Technol.*, 2010, **44**(20), 7749–7755.
4 A. K. S. Samuel, S. R. Dasary, D. Senapati, H. Yu and P. C. Ray, *J. Am. Chem. Soc.*, 2009, **131**, 13806–13812.
5 N. A. Hatab, G. Eres, P. B. Hatzinger and B. Gu, *J. Raman Spectrosc.*, 2010, **41**, 1131–1136.
6 P. R. West, S. Ishii, G. V. Naik, N. K. Emani, V. M. Shalaev and A. Boltasseva, *Laser Photonics Rev.*, 2010, **4**, 795–808.
7 F. Avila, D. J. Fernandez, J. F. Arenas, J. C. Otero and J. Soto, *Chem. Commun.*, 2011, **47**, 4210–4212.
8 W. E. Smith, *Chem. Soc. Rev.*, 2008, **37**, 955–964.
9 K. L. Wustholz, C. L. Brosseau, F. Casadio and R. P. Van Duyne, *Phys. Chem. Chem. Phys.*, 2009, **11**, 7350–7359.
10 M. A. Y. George, C. Schatz and R. P. Van Duyne, *Top. Appl. Phys.*, 2009, **103**, 19–46.
11 F. Büttner, J. Hagemann, M. Wellhausen, S. Funke, C. Lenth, F. Rotter, L. Gundrum, U. Plachetka, C. Moormann, M. Strube, A. Walte and H. Wackerbarth, *SPIE Security and Defence*, International Society for Optics and Photonics, 2013.
12 I. Talian and J. Huebner, *J. Raman Spectrosc.*, 2013, **44**, 536–539.
13 K. A. Mahmoud and M. Zourob, *Analyst*, 2013, **138**, 2712–2719.
14 A. K. M. Jamil, E. L. Izake, A. Sivanesan, R. Agoston and G. A. Ayoko, *Anal. Methods*, 2015, **7**, 3863–3868.
15 M. Liu and W. Chen, *Biosens. Bioelectron.*, 2013, **46**, 68–73.
16 T. Demeritte, R. Kanchanapally, Z. Fan, A. K. Singh, D. Senapati, M. Dubey, E. Zakar and P. C. Ray, *Analyst*, 2012, **137**, 5041–5045.
17 S. L. Kleinman, B. Sharma, M. G. Blaber, A.-I. Henry, N. Valley, R. G. Freeman, M. J. Natan, G. C. Schatz and R. P. Van Duyne, *J. Am. Chem. Soc.*, 2013, **135**, 301–308.
18 T. Chen, S. Lu, A. Wang, D. Zheng, Z. Wu and Y. Wang, *Appl. Surf. Sci.*, 2014, **317**, 940–945.
19 M. K. Khaing Oo, C.-F. Chang, Y. Sun and X. Fan, *Analyst*, 2011, **136**, 2811–2817.
20 M. K. K. Oo, C.-F. Chang, Y. Sun and X. Fan, *Analyst*, 2011, **136**, 2811–2817.
21 S. Emamian, A. Eshkeiti, B. B. Narakathu, S. G. Avuthu and M. Z. Atashbar, in *SENSORS, 2014 IEEE*, IEEE Xplore, Valencia, Spain, 2014, pp. 1069–1072, DOI: 10.1109/ICSENS.2014.6985189.
22 S. Tamane, Ç. Ö. Topal and A. K. Kalkan, Vapor phase SERS sensor for explosives detection, in *Nanotechnology (IEEE-NANO), 2011 11th IEEE Conference*, IEEE Xplore, Portland, OR, USA, 2011, pp. 301–306, DOI: 10.1109/NANO.2011.6144447.
23 S. Ben-Jaber, W. J. Peveler, R. Quesada-Cabrera, E. Cortes, C. Sotelo-Vazquez, N. Abdul-Karim, S. A. Maier and I. P. Parkin, *Nat. Commun.*, 2016, **7**, 12189.
24 P. H. Camargo, L. Au, M. Rycenga, W. Li and Y. Xia, *Chem. Phys. Lett.*, 2010, **484**, 304–308.
25 K. Kneipp, H. Kneipp and J. Kneipp, *Acc. Chem. Res*, 2006, **39**, 443–450.
26 E. C. Le Ru, M. Meyer, E. Blackie and P. G. Etchegoin, *J. Raman Spectrosc.*, 2008, **39**, 1127–1134.
27 E. C. Le Ru, P. G. Etchegoin and M. Meyer, *J. Chem. Phys.*, 2006, **125**, 204701.
28 S. Botti, L. Cantarini, S. Almaviva, A. Puiu and A. Rufoloni, *Chem. Phys. Lett.*, 2014, **592**, 277–281.
29 P. H. Camargo, M. Rycenga, L. Au and Y. Xia, *Angew. Chem., Int. Ed.*, 2009, **48**, 2180–2184.
30 P. H. Camargo, L. Au, M. Rycenga, W. Li and Y. Xia, *Chem. Phys. Lett.*, 2010, **484**, 304–308.
31 P. H. Camargo, C. M. Cobley, M. Rycenga and Y. Xia, *Nanotechnology*, 2009, **20**, 434020.
32 C. L. Zhang, K. P. Lv, H. P. Cong and S. H. Yu, *Small*, 2012, **8**, 648–653.

33 S. Y. Lee, L. Hung, G. S. Lang, J. E. Cornett, I. D. Mayergoyz and O. Rabin, *ACS Nano*, 2010, **4**, 5763–5772.
34 Q. Fu, D. Zhang, Y. Chen, X. Wang, L. Han, L. Zhu, P. Wang and H. Ming, *Appl. Phys. Lett.*, 2013, **103**, 041122.
35 M. Rycenga, M. H. Kim, P. H. Camargo, C. Cobley, Z.-Y. Li and Y. Xia, *J. Phys. Chem. A*, 2009, **113**, 3932–3939.
36 B. Wang, L. Zhang and X. Zhou, *Spectrochim. Acta, Part A*, 2014, **121**, 63–69.
37 R. Kodiyath, S. T. Malak, Z. A. Combs, T. Koenig, M. A. Mahmoud, M. A. El-Sayed and V. V. Tsukruk, *J. Mater. Chem. A*, 2013, **1**, 2777–2788.
38 S. Emamian, A. Eshkeiti, B. B. Narakathu, S. G. R. Avuthu and M. Z. Atashbar, *Sens. Actuators, B*, 2014, **217**, 129–135.
39 H. Östmark, S. Wallin and H. G. Ang, *Proppell. Explos. Pyrot.*, 2012, **37**, 12–23.
40 S. Bell, *Forensic chemistry*, Pearson Prentice Hall, Upper Saddle River, N.J., 2006.
41 Z.-Q. Tian, Z.-L. Yang, B. Ren, J.-F. Li, Y. Zhang, X.-F. Lin, J.-W. Hu and D.-Y. Wu, *Faraday Discuss.*, 2006, **132**, 159–170.
42 S. E. Skrabalak, L. Au, X. Li and Y. Xia, *Nat. Protocols*, 2007, **2**, 2182–2190.
43 D. Chen, G. Zhu, X. Zhu, X. Qiao and J. Chen, *J. Mater. Sci.: Mater. Electron.*, 2011, **22**(12), 1788–1795.
44 E. C. Le Ru, E. Blackie, M. Meyer and P. G. Etchegoin, *J. Am. Chem. Soc.*, 2007, **111**, 13794–13803.
45 M. Rycenga, M. H. Kim, P. H. C. Camargo, C. Cobley, Z. Y. Li and Y. Xia, *J. Chem. Phys. A*, 2009, **113**, 3932–3939.
46 F. Calzzani Jr., R. Sileshi, A. Kassu, J. M. Taguenang, A. Chowdhury, A. Sharma, P. Ruffin, C. Brantley and E. Edwards, SPIE Defense and Security Symposium, 2008.
47 M. Liu and W. Chen, *Biosens. Bioelectron.*, 2013, **46**, 68–73.
48 R. G. Ewing, M. J. Waltman, D. A. Atkinson, J. W. Grate and P. J. Hotchkiss, *TrAC, Trends Anal. Chem.*, 2013, **42**, 35–48.